

Title	Amplitude-modulated cavity-enhanced absorption spectroscopy with phase-sensitive detection: A new approach applied to the fast and sensitive detection of NO ₂
Authors	Zhou, Jiacheng;Zhao, Weixiong;Zhang, Yang;Fang, Bo;Cheng, Feihu;Xu, Xuezhe;Ni, Shichuan;Zhang, Weijun;Ye, Chunxiang;Chen, Weidong;Venables, Dean S.
Publication date	2022-02-10
Original Citation	Zhou, J., Zhao, W., Zhang, Y., Fang, B., Cheng, F., Xu, X., Ni, S., Zhang, W., Ye, C., Chen, W. and Venables, D. S. (2021) 'Amplitude-modulated cavity-enhanced absorption spectroscopy with phase-sensitive detection: A new approach applied to the fast and sensitive detection of NO ₂ ', <i>Analytical Chemistry</i> , 94(7), pp. 3368-3375. doi: 10.1021/acs.analchem.1c05484
Type of publication	Article (peer-reviewed)
Link to publisher's version	10.1021/acs.analchem.1c05484
Rights	© 2022, American Chemical Society. This document is the Accepted Manuscript version of a Published Work that appeared in final form in <i>Analytical Chemistry</i> , after technical editing by the publisher. To access the final edited and published work see: https://doi.org/10.1021/acs.analchem.1c05484
Download date	2025-04-20 03:11:38
Item downloaded from	https://hdl.handle.net/10468/12711



UCC

University College Cork, Ireland
Coláiste na hOllscoile Corcaigh

Amplitude modulated cavity enhanced absorption spectroscopy with phase-sensitive detection: a new approach applied to fast and sensitive detection of NO₂

Jiacheng Zhou,^{†,‡} Weixiong Zhao,^{*,†} Yang Zhang,[†] Bo Fang,[†] Feihu Cheng,[†] Xuezhe Xu,[†] Shichuan Ni,^{†,‡} Weijun Zhang,^{*,†,‡} Chunxiang Ye,[§] Weidong Chen,^{//} Dean S. Venables[⊥]

[†] Laboratory of Atmospheric Physico-Chemistry, Anhui Institute of Optics and Fine Mechanics, HFIPS, Chinese Academy of Sciences, Hefei 230031, Anhui, China

[‡] University of Science and Technology of China, Hefei 230026, Anhui, China

[§] College of Environmental Sciences and Engineering, Peking University, Beijing 100871, China

^{//} Laboratoire de Physicochimie de l'Atmosphère, Université du Littoral Côte d'Opale, 59140 Dunkerque, France

[⊥] School of Chemistry and Environmental Research Institute, University College Cork, Cork T23 XE10, Ireland

ABSTRACT: Accurate and sensitive measurements of NO₂ play an extremely important role in atmospheric studies. Increasingly, studies require NO₂ measurements with pptv-level (parts per trillion by volume) detection limits. Other desirable instrument attributes include easy of use, long-term stability, and low maintenance. In this work, we report the development of an Amplitude Modulated multimode-diode-laser-based Cavity Enhanced Absorption Spectroscopy (AM-CEAS) system operating at 406 nm that uses phase-sensitive detection for extremely sensitive NO₂ detection. The laser was TTL modulated at 35 kHz. The mirror reflectivity was determined to be 99.985% based on the ring-down time measurement. The cavity base length was 47.5 cm, giving an effective absorption pathlength of ~ 3.26 km. AM-CEAS achieved a 1 σ detection precision of 35 pptv in a 1 s data acquisition time (4.98×10^{-10} cm⁻¹), over 4 times lower than that attained using a ring-down approach and the same optical system. The AM-CEAS precision improved to 8 pptv over a data acquisition time of 30 s (1.14×10^{-10} cm⁻¹). The AM-CEAS method with the multimode diode laser integrates the advantages of high light injection efficiency like on-axis alignment cavity ring-down spectroscopy (CRDS), low cavity mode noise like off-axis alignment CEAS and narrow bandwidth high-sensitivity weak signal detection of modulation spectroscopy, providing a powerful, straightforward, and general method for ultra-sensitive absorption and extinction measurements.

Nitrogen dioxide (NO₂) is one of the most important molecules in the formation of ozone (O₃), acid deposition, and secondary particulate pollutants, and has a profound impact on human health, the environment and climate change.¹⁻⁴ In the past 20 years, high sensitivity, precision, and accurate NO₂ detection technology has developed rapidly, especially optical methods based on high-finesse cavities.^{5,6} In tandem with chemical conversion, NO₂ measurements can also be used to measure a range of other important reactive atmospheric species. For example, thermal dissociation followed by NO₂ detection can be used for precision measurement of total reactive nitrogen, including total peroxy nitrate (Σ PNs), total alkyl nitrate (Σ ANs), and nitric acid (HNO₃).⁷⁻¹⁴ Likewise, the chemical amplification method can be used to measure total peroxy radicals,¹⁵⁻¹⁹ while titration of the inlet stream allows O₃ and nitric oxide (NO) to be quantified.^{13,20,21} In short, sensitive NO₂ detection approaches have enhanced our understanding of nitrogen chemistry, free radical chemistry, and atmospheric oxidation capacity.²²⁻²⁴

With NO₂'s strong absorption between 400 – 480 nm, most cavity-based instruments currently operate in the visible spectral range.²⁵ The reported methods include cavity ring-down spectroscopy (CRDS),^{8-10,12,13,15,16,20,21,26} cavity attenuated phase shift spectroscopy (CAPS),^{11,18,27} cavity-enhanced spectroscopy (CEAS),²⁸ optical feedback cavity-enhanced absorption spectroscopy (OF-CEAS),^{17,29} mode-locked cavity-enhanced absorption spectroscopy (ML-CEAS),³⁰ and broadband cavity-enhanced absorption spectroscopy (BBCEAS).^{6,14,19,31}

CAPS and BBCEAS methods use incoherent light sources (Xe arc lamp or LEDs) and do not require the light beam to be strictly matched to the spatial mode of the cavity TEM₀₀ mode, helping make these instruments simple, robust, and highly suited to field applications.⁶ In contrast, laser-based cavity spectroscopy techniques³² generally require on-axis optical alignment to improve laser injection efficiency into the cavity to achieve better performance.³³ The system must have high mechanical stability. The best performance can be realized by using cavity/laser locking techniques,^{32,34,35} but this approach undoubtedly increases system complexity.

In addition to injection efficiency, cavity mode noise is also a key factor that limits detection sensitivity.³⁶ With off-axis (OA) alignment, an extremely dense-mode spectrum of the cavity is created, which greatly reduces cavity mode noise. In this case, the cavity acts more like a traditional optical multipass cell with a flat transmission spectrum.³⁶⁻³⁸ However, this non-resonant coupling scheme limits the use of ultra-high reflectivity mirrors because light injection efficiency is low, precluding large increases in the absorption pathlength to improve the detection sensitivity. To obtain a high signal-to-noise ratio, a trade-off must be made between the mirror reflectivity and cavity transmission intensity.

The recently developed multimode-diode-laser-based CRDS^{10,20,39} uses a broadband Fabry-Perot (FP) diode laser (with a line width of ~ 0.5 nm), which can simultaneously excite thousands of cavity modes, thus avoiding the need for mode matching between the laser and the cavity. Taking a 406 nm

laser as an example, the spectral range of a 0.5 nm laser line width is ~ 900 GHz, while the free spectral range of the optical cavity is generally 200 – 400 MHz. As a result, roughly 2000 – 4500 cavity modes occur across the laser line width. The slight mode changes have negligible impact on the laser injection. The system is aligned on-axis and has a high and stable injection efficiency without the need for complex electronic control. At the same time, cavity mode noise is effectively suppressed. This effect is similar to that achieved by off-axis alignment. These advantages greatly simplify the CRDS instrument. Using a 40 mW F-P diode laser with a center wavelength of 404 nm, Fuchs et al.²⁰ achieved a NO₂ detection limit of 11 pptv (1 σ , 1s) with mirror reflectivity R of $\sim 99.9965\%$ (with ring-down time $\tau_0 > 44 \mu\text{s}$). Thieser et al.¹⁰ reported a NO₂ detection limit of 28 pptv (1 σ , 1s) with a 120 mW diode laser centered at 405 nm ($R \sim 99.9965\%$, $\tau_0 = 38 \mu\text{s}$). In the case of further increasing the laser power to ~ 1.1 W, Karpf et al.³⁹ achieved a detection limit of 38 pptv with an integration time of 128 ms at a wavelength of 400 nm ($R \sim 99.97\%$, $\tau_0 \sim 5.6 \mu\text{s}$).

In this work, we report the development of an Amplitude Modulated multimode-diode-laser-based CEAS (AM-CEAS) operating at 406 nm for high-sensitivity NO₂ detection. Combined with phase-sensitive detection,^{36,40} a detection limit of 35 pptv (1 σ , 1s) was achieved with $R \sim 99.985\%$ ($\tau_0 \sim 10.87 \mu\text{s}$). The sensitivity of AM-CEAS was a factor of 4 better than that achieved using a CRDS scheme with the same experimental setup (157 pptv). The AM-CEAS method combines the advantages of high injection efficiency like on-axis alignment CRDS, low cavity mode noise like off-axis CEAS, and the narrow bandwidth, high-sensitivity detection of modulation spectroscopy, providing a simple yet powerful method for sensitive absorption and extinction measurements in a high finesse cavity.

EXPERIMENTAL SECTION

Experimental Setup. The experimental setup of the AM-CEAS is depicted in Figure 1. The light source used was a continuous wave (CW) operation free space matchbox diode laser module (0405L-11A-NI-NT-NF, Integrated Optics, TEM₀₀ transverse mode, multiple longitudinal mode). The diode module used a 5 V power supply and delivered an output power of ~ 150 mW with a central wavelength of 406 nm and 0.4 nm spectral line width. Internal temperature stability was maintained by a TEC installed on a heat sink. The integrated precision temperature and current control drivers ensured low-noise and stable operation across a wide temperature range. The light intensity stability was better than 0.4%. The laser, which can be modulated up to 10 MHz by an external TTL signal, had a rise time of 14.4 ns and a fall time of 28.4 ns. The laser beam was then coupled into the high finesse optical cavity. An optical isolator (IO-3D-405-PBS, Thorlabs) was placed between the laser and the cavity to minimize optical feedback. Light transmitted through the cavity was detected with a photomultiplier tube (PMT, H14600-20, Hamamatsu). In front of the PMT, a band-pass filter (FB405-10, Thorlabs), centered at 405 nm with an FWHM (full width at half-maximum) of 10 nm, was used to eliminate ambient stray light.

The optical layout was similar to our previous BBCEAS instrument, with a custom cage design and a footprint of 74 mm by 676 mm.³¹ The cavity was made of a PFA (perfluoroalkoxy) tube with 9 mm inner diameter. The distance between the two high reflectivity mirrors (Layertec, 25 mm diameter, 1 m radius

of curvature, $R \sim 99.98\%$ at 406 nm) was 47.5 cm. The mirrors were not purged to prevent the mirror reflectivity degradation because a Teflon filter (Parker, Balston) in the inlet removed particles from the sample stream. The sample flow rate was 1.5 L/min and the residence time in the cavity was about 1.4 s.

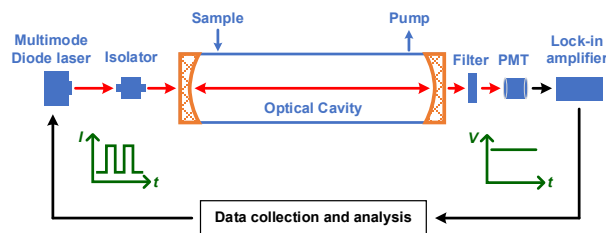


Figure 1. Schematic diagram of the experimental setup of the AM-CEAS instrument.

Square Wave Amplitude Modulation and Phase-Sensitive Detection. The phase sensitive detector (PSD) is a multiplier that provides a powerful and simple method for weak signal detection.^{41,42} The principal block diagram is shown in Figure 2. The most commonly used PSD device is a lock-in amplifier. It mixes the signal (V_{sig}) with a reference (V_{ref}) to give an output of the product ($V_{sig} \times V_{ref}$). Then the signal at a frequency of interest (V_{psd}) is selected within a narrow bandwidth by using a low pass filter (RC filter). Using PSD, signals can be measured accurately even when the magnitude of the signal is thousands of times smaller than that of the noise.

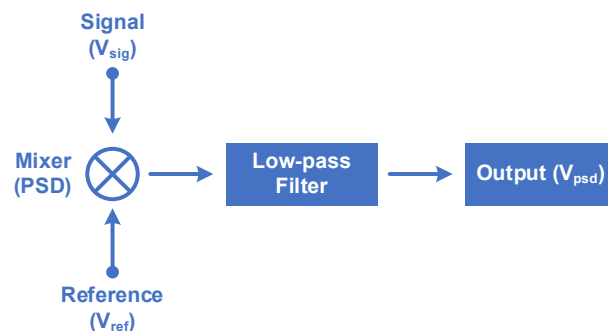


Figure 2. Principle block diagram of the phase sensitive detection (PSD).

TTL modulation is based on square wave pulses with alternating low and high voltages. The high voltage signal turns on the laser (100% of the laser power is emitted) and the low voltage signal turns off the laser. The light intensity waveform of the TTL modulated laser $V_s(t)$ can be represented by a Fourier series of many sine waves at odd multiples of f_m , the modulation frequency:

$$V_s(t) = \frac{V_{sig}}{2} + \frac{2V_{sig}}{\pi} \sum_{n=0}^{\infty} \frac{1}{(2n+1)} \sin[(2n+1)2\pi f_m t + \theta_{sig}] \quad (1)$$

where V_{sig} is the laser output power and θ_{sig} is the signal's phase. When the reference frequency is locked to f_m (with a reference signal of $V_{ref} \sin(2\pi f_m t + \theta_{ref})$, where V_{ref} is the amplitude and θ_{ref} is the phase of the reference), only the first harmonic is singled out with $1f$ -harmonic detection. The filtered output of the PSD is:

$$V_{psd} = \frac{V_{sig}}{\pi} V_{ref} \cos \theta \quad (2)$$

where $\theta = \theta_{sig} - \theta_{ref}$, is the difference between θ_{sig} and θ_{ref} . V_{psd} is therefore proportional to the laser transmission intensity (I) through the cavity and can be directly used for cavity-enhanced measurement. The schematic diagrams of the different signals are illustrated in Figure 3. In this work, a SR830 dual-phase lock-in amplifier was used for the phase-sensitive detection. To remove the phase dependence, the amplitude of the signal ($(X^2+Y^2)^{1/2}$) was measured directly instead of measuring the “in-phase” (X) or “quadrature” (Y) components. The approach presented here of measuring the signal amplitude of the cavity transmitted light differs from the CAPS approach,²⁷ which measures the phase shift of the modulated light transmitted through the cavity. In addition, in CAPS, the modulation frequency is usually chosen so that the phase shift of the empty cavity is equal to 45°. Matching the modulation frequency and the phase shift is not necessary in our approach.

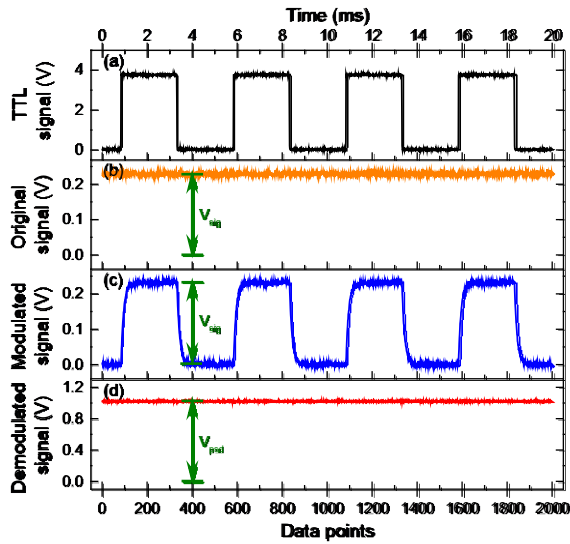


Figure 3. (a) TTL signal; transmission intensity of the cavity (b) without modulation and (c) with TTL modulation of the cw operation diode laser; and (d) the demodulated output signal of (c) with phase-sensitive detection.

To select an appropriate frequency for amplitude modulation and phase-sensitive detection to achieve a low detection limit, the frequency dependent noise of the system was recorded with a signal analyzer (N9000A CXA, Keysight Technologies). The bandwidth of the analyzer limited the lowest frequency to 9 kHz. The results are shown in Figure 4. An InGaAs photodetector was used to directly measure the laser intensity (here the laser was not injected into the cavity) for the laser noise analysis. Below 70 kHz, laser intensity noise (black hollow circles in the figure) increased slightly as the frequency increased. For frequencies larger than 70 kHz, the laser intensity noise decreased as the frequency increased, which showed a clear $1/f$ dependence.⁴³

The total intensity noise transmitted through the cavity was recorded by the PMT (red solid diamonds in the figure). By turning off the laser, the noise from the PMT can be distinguished (blue solid circles in the figure). Both the PMT and the total intensity noise showed clear spikes at some frequencies, which may be caused by electronic noise from the PMT cir-

cuitry. The values of these peaks were similar, but the frequencies were shifted when the laser was on. An indication of cavity mode noise was obtained by removing these peaks and subtracting the laser and PMT noises from the total noise. When the frequency was lower than 50 kHz, this noise (green hollow diamonds in the figure) decreased as frequency rose and it was smaller than laser noise between 30 kHz and 70 kHz.

In general, in the frequency range of 33 to 59 kHz, the total intensity noise level was relatively low and flat. Therefore, a modulation frequency of 35 kHz was chosen in this work. The performance at higher frequencies was not tested owing to the limited bandwidth of the detector and the noise spikes at higher frequencies.

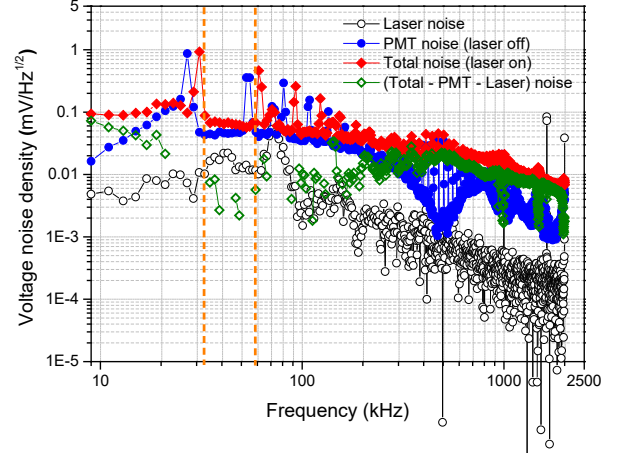


Figure 4. Frequency dependent noise spectrum of the laser, the PMT and the total noise of the AM-CEAS system. The light intensity noise transmitted through the cavity was measured by subtracting the laser and PMT noise from the total noise after masking noise spikes.

Cavity-enhanced measurement. CEAS is based on the measurement of light intensities transmitted through the cavity with (I) and without (I_0) samples:

$$\alpha = n\sigma = \left(\frac{1-R}{L}\right) \left(\frac{I_0}{I} - 1\right), \quad (3)$$

where n and σ are the number density and absorption or extinction cross section of the sample, respectively. L is the distance between two high reflectivity mirrors and R is the mirror reflectivity. The mirror reflectivity R must be experimentally determined for quantitative detection.⁴⁴

The laser was TTL modulated. When the laser was turned on, light intensity in the cavity built up rapidly; when the laser was turned off (at the falling edge of the TTL), the light intensity in the cavity decayed rapidly and exponentially (as shown in Figure 5). To determine the mirror reflectivity R , the ring-down time (τ) in the cavity was determined by fitting the exponential decay:

$$\frac{1-R}{L} = \frac{1}{c\tau_0}, \quad (4)$$

where τ_0 is the ring-down time without absorbing sample in the cavity and c is the speed of light.

For AM-CEAS detection, equation 3 can be rewritten as follows:

$$\alpha = \frac{1}{c\tau_0} \left(\frac{V_{psd-0}}{V_{psd}} - 1\right), \quad (5)$$

where V_{psd} and V_{psd_0} are the demodulated output signals of the PSD with and without samples.

A typical ring-down measurement is shown in Figure 5. The laser was modulated at 5 kHz. The measured τ_0 was 10.87 μs , which corresponded to a mirror loss $(1-R)$ of 145.7 ppm ($R = 99.985\%$) for a 47.5 cm long cell and an effective absorption pathlength of 3.26 km. Since τ_0 and I_0 can be obtained periodically by flushing the cavity with zero air, the AM-CEAS system has the advantage of a straightforward and reliable self-calibration method for quantitative extinction measurements. In fact, under low TTL modulation frequencies, since light intensities and the CRDS signals can be recorded simultaneously, both CEAS and CRDS detection can be realized in the same experimental setup at the same time without the need for additional optical or electronic switching (as shown in Figures 3 and 5).

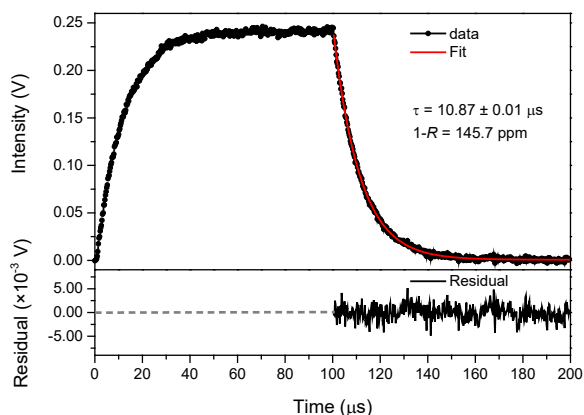


Figure 5. A typical cavity ring-down measurement to determine the mirror reflectivity. Upper panel: signal of the TTL modulated diode laser. At the falling edge of the TTL, the laser was rapidly switched off and the ring-down time was determined by fitting the exponential decay. The lower panel shows the fit residual.

RESULTS AND DISCUSSION

Laboratory test: The results of the AM-CEAS measurement were validated by CRDS measurements of laboratory generated diluted samples of NO_2 (Figure 6). The laser was TTL modulated at 5 kHz. The signals of AM-CEAS and CRDS were measured simultaneously. Different concentrations of NO_2 in N_2 were prepared by flow dilution of a 10 ppmv reference NO_2/N_2 mixture. The cavity was flushed with N_2 between different concentration measurements. The time profile of the measurement is shown in Figure 6(a), and the corresponding correlation plot between AM-CEAS and CRDS measurements is shown in Figure 6(b). The slope, intercept and correlation coefficient for the comparison were 1.01, 0.12 ppbv and 0.99, respectively. These results indicate excellent agreement between AM-CEAS and the well-established CRDS technique, demonstrating that AM-CEAS produces sensitive and accurate measurements of NO_2 and, more generally, of sample extinction.

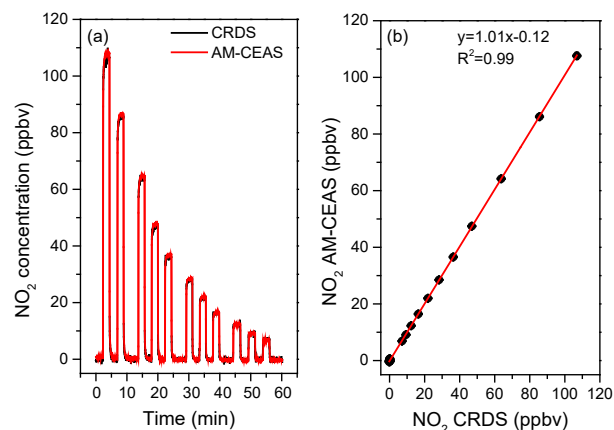


Figure 6. Comparison of NO_2 measurement by AM-CEAS and CRDS with the same experimental setup. (a) Time profile of NO_2 concentration of diluted sample streams. (b) Correlation of the NO_2 concentration measurements by AM-CEAS and CRDS.

Precision and Accuracy: The laser emission spectrum provided by the manufacturer (measured with an Optical Spectrum Analyzer (OSA) with a resolution of 20 pm), and the absorption cross section spectra of NO_2 , glyoxal and methylglyoxal respectively reported by Vandaele et al.,⁴⁵ Volkamer et al.,⁴⁶ and Meller et al.,⁴⁷ are shown in Figure 7. The effective absorption cross-section of NO_2 ($5.74 \times 10^{-19} \text{ cm}^2/\text{molecule}$) was determined by the average value of high-resolution NO_2 spectrum in the spectral width of the laser emission (405.7 nm to 406.15 nm).¹⁰ The NO_2 cross section at 405 nm is about an order of magnitude larger than that of glyoxal and methylglyoxal. In addition, the environmental concentrations of these compounds (about 1 ppbv in polluted atmosphere, and smaller than 100 pptv in clean air) are generally much lower than that of NO_2 . As a result, the interference arising from absorption by these dicarbonyl compounds will be a negligible ($< 1\%$) fraction of atmospheric NO_2 concentrations under most circumstances.⁴⁸

As the inlet loss of NO_2 in the PFA tube was negligible,⁴⁹ the accuracy of NO_2 detection by AM-CEAS is mainly determined by the uncertainty in the magnitude of the literature reference cross section ($\sim 1\%$), the uncertainty in the appropriate absorption cross section to use arising from uncertainty in the laser output wavelength spectrum ($\sim 5\%$), and the uncertainty in the ring-down measurement of R ($\sim 1\%$). The total uncertainty (summed in quadrature) of NO_2 measurement with AM-CEAS was estimated to be better than 6%.

The error in the absorption cross section of NO_2 was the dominant uncertainty. The value of 5% uncertainty reported here was the upper limit of the difference between the averaged absorption cross-section over the laser spectral width compared with the entire laser emission spectral range, from 405.3 nm to 406.2 nm. Fuchs et al.²⁰ reported that by measuring known concentrations of NO_2 to determine the effective absorption cross-section of NO_2 , the error was reduced to 3%. Since the effective cross-section of NO_2 was the main limiting factor, a similar approach could be taken here to further improve the accuracy of the instrument.

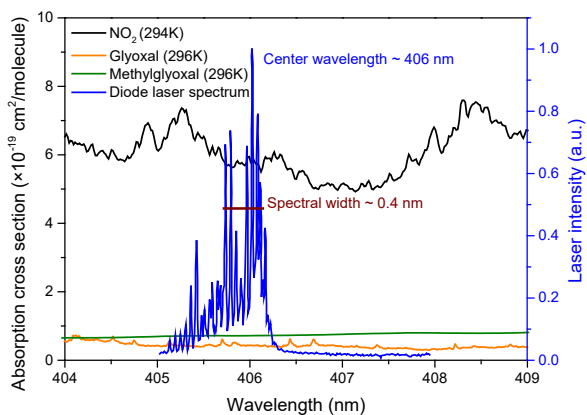


Figure 7. Emission spectrum of the laser diode (adapted from the manufacturer test report) and the absorption cross section spectra of NO₂, glyoxal and methylglyoxal at ambient pressure.

The precision and stability of AM-CEAS method were investigated using Allan variance analysis, as shown in Figure 8. The performance of the AM-CEAS was evaluated at two different modulation frequencies ($f_m = 5$ kHz and 35 kHz). For comparison, CRDS measurement results at $f_m = 5$ kHz were also recorded. As the repetition rate of 35 kHz is too fast to build up light intensity in the cavity, CRDS measurement at $f_m = 35$ kHz was not implemented.

The time series measurement and the corresponding Allan deviation are shown in Figure 8. For a 1 s data acquisition time, the precisions of CRDS and AM-CEAS at $f_m = 5$ kHz (AM-CEAS-5kHz) and 35 kHz (AM-CEAS-35kHz) were 157 pptv, 57 pptv and 35 pptv, respectively. The corresponding extinction sensitivities were 2.24×10^{-9} cm⁻¹, 8.12×10^{-10} cm⁻¹ and 4.98×10^{-10} cm⁻¹, respectively. The performance of the present instrument with mirrors of $R \sim 99.985\%$ is comparable to the state-of-the-art performance (28 pptv in 1 s) demonstrated by Thieser et al. using CRDS with mirrors of $R \sim 99.9965\%$.¹⁰

The precision of AM-CEAS at 35 kHz was about two times better than that at 5 kHz and the long-term stability was also improved. Although the signal analyzer could not measure the noise at 5 kHz, the difference in precision at the two modulation frequencies is consistent with the noise measurement shown in Figure 4. The low noise level at 35 kHz helped to improve the signal-to-noise ratio, which was 1.6 times better at 35 kHz than at 5 kHz at 1 s integration time. When the integration time was extended to 30 s, the NO₂ measurement precision of AM-CEAS at 35 kHz improved to 8 pptv (equivalent to 1.14×10^{-10} cm⁻¹ extinction measurement); this precision is 5 times better than the 42 pptv achieved by our CRDS measurement over the same time period.

The frequency distribution of the time series measurement of NO₂ with AM-CEAS and CRDS is shown in the lower panel of Figure 8. The absolute offsets and standard deviations of the histograms represent the background and actual instrument precision of the developed instrument.³¹ Obviously, the AM-CEAS method significantly improved the performance of the instrument.

The results show the advantages of AM-CEAS. Since the PSD method can effectively filter out noise, it has obvious advantages in weak signal detection. We expect that with higher reflectivity mirrors the detection sensitivity will continue to increase with the longer light absorption pathlength in the optical cavity, even though the light transmission intensity decreases.

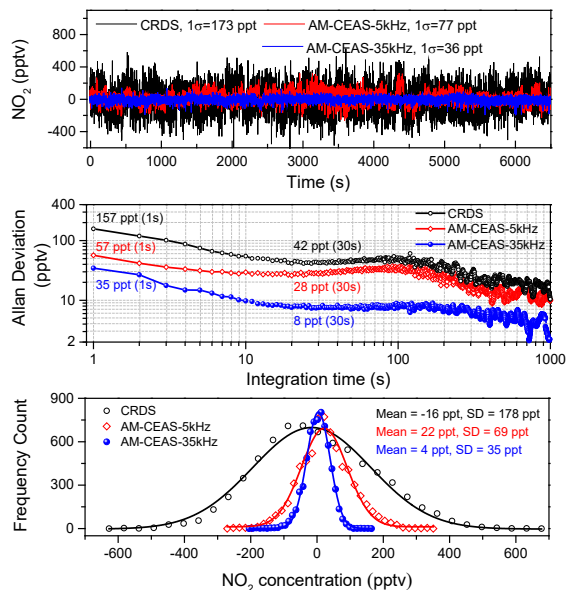


Figure 8. Performance evaluation of the AM-CEAS method. Upper panel: time series measurement of NO₂ concentration in zero air with AM-CEAS (at modulation frequencies of 5 kHz and 35 kHz) and CRDS recorded with a repetition rate of 5 kHz. Middle and lower panels are the corresponding Allan deviation plot and the frequency distribution of the time series measurement.

Ambient application: Validation of the AM-CEAS method for ambient air measurements was carried out at the office building of Anhui Institute of Optics and Fine Mechanics (31°54'18"N, 117°9'42"E) over the period 28 – 30 October 2021. The results were compared with a BBCEAS instrument. A detailed description of the BBCEAS instrument for NO₂ measurement can be found in Fang et al.³¹ The instrument used a blue LED as light source and detected NO₂ across the spectral range of 440–480 nm. The detection limit was about 40 pptv in a 1 s integration time with an accuracy about 4% (mainly influenced by uncertainties in the literature reported absorption cross-section of NO₂ (1%), and the Rayleigh scattering cross-sections of CO₂ (4%) and N₂ (1%) used in the calibration of mirror reflectivity). Importantly, for the purposes of this comparison, the BBCEAS measurement is based on the highly structured spectrum of NO₂ across multiple wavelengths, giving the method high specificity to NO₂ and low susceptibility to interferences arising from the absorption or scattering of other atmospheric constituents.

Instruments were located in a laboratory and ambient air was sampled through a FEP tube with an inlet about 6 m above the ground level. The site is located on a peninsula, surrounded by water on three sides, about 15 km west of the downtown center of Hefei city (population 8.0 million). There are no obvious industrial emission sources within 6 km. A time series measurement with AM-CEAS, CRDS and BBCEAS are shown in Figure 9. During the 47 hours observation period, high levels of NO₂ occurred in the morning and evening rush hours. Both the AM-CEAS / CRDS and BBCEAS instruments have a good time response to rapid concentration changes, mostly likely caused by traffic emissions from cars and buses.

The deviation between AM-CEAS and CRDS was about 3%. This was higher than that in the laboratory test, which may be caused by the duty cycle in the CRDS measurement. Due to the rapid changes in NO₂ concentrations during the measurement

period, the duty cycle may cause some concentration changes that cannot be captured, resulting in small concentration deviations. The values of AM-CEAS/CRDS were smaller than that of BBCEAS, especially at low NO_2 concentrations. Different inlet losses between the instruments, or an overestimation in the effective absorption cross-section used in the AM-CEAS and CRDS measurements could account for the higher reported concentrations. Absorption or scattering by other atmospheric constituents (such as glyoxal and methylglyoxal) would also result

in higher values measured by the AM-CEAS and CRDS instruments.

In summary, these ambient air measurements with NO_2 concentrations varying by an order of magnitude show excellent agreement between the different methods. These results demonstrate the high performance of the AM-CEAS method and its potential for field application.

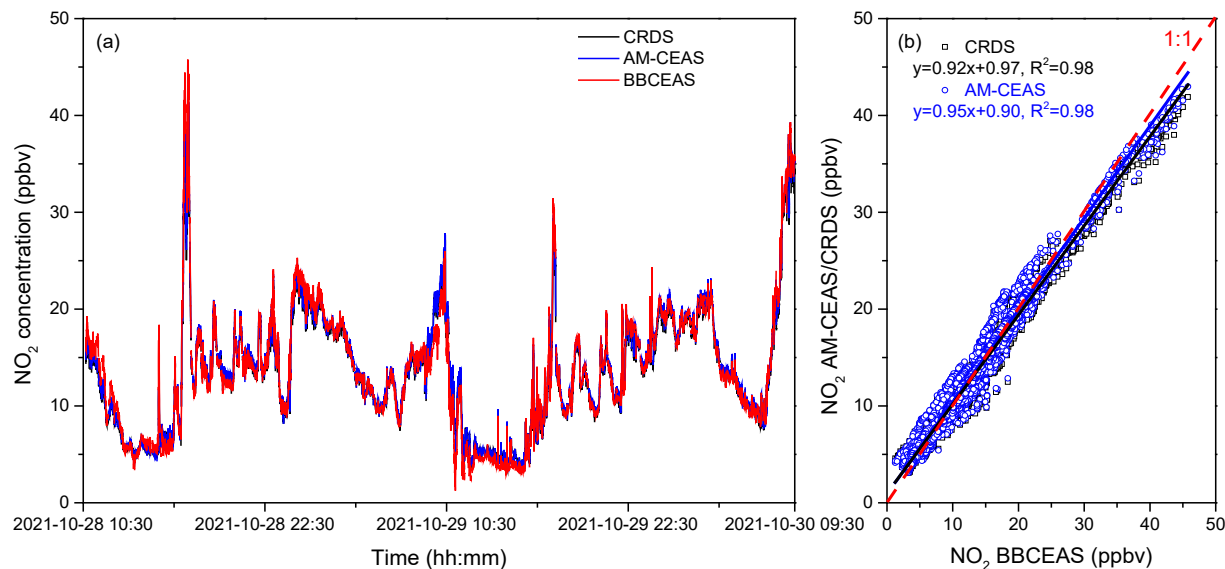


Figure 9. Comparison of ambient NO_2 measurement with AM-CEAS, CRDS and BBCEAS. (a) Time series measurement, and (b) correlation plot of the AM-CEAS and CRDS measurements against the BBCEAS measurements. All data were acquired at a time resolution of 10 s.

CONCLUSIONS

Broadband multimode-diode-laser based cavity spectroscopy simplifies the instrument by avoiding the need for mode matching between the laser and the cavity, high mechanical stability, and complex electronic control. This approach will not suit all applications. One shortcoming is that it is not suitable for studying molecules with narrower spectral features than the broadband output of the laser. A second consideration is that detection is at a single wavelength. Unlike wavelength-resolved measurement methods, such as BBCEAS, measurement of sample extinction at a single wavelength cannot realize simultaneous measurement of multiple species, and attention must be paid to the potential interferences arising from the absorption or scattering of other atmospheric constituents. Nevertheless, these limitations must be placed in context: for dominant absorbers, such as NO_2 in this work, the sensitivity and precision of the approach are competitive and attractive.

Phase-sensitive detection retrieves the signal in an extremely narrow bandwidth and can effectively filter out most noise, giving rise to a powerful and straightforward method for detecting weak absorption or extinction signals. In this work, we combined these two technologies. We report the development of an amplitude modulated multimode-diode-laser-based CEAS in-

strument which operated at 406 nm for ultra-high-sensitivity detection of the major air pollutant NO_2 . A detection precision of 8 pptv (1σ , 30s) was achieved with an effective absorption path-length of ~ 3.26 km ($R \sim 99.985\%$). By selecting the modulation and demodulation frequency in a low noise level region of the noise spectrum, the precision can be effectively improved. As PSD has the advantages of weak signal detection, we expected that higher detection sensitivity can be achieved using higher reflectivity mirrors.

AM-CEAS integrates the advantages of high injection efficiency, low cavity mode noise, and narrow bandwidth for high-sensitivity detection of weak signals. It provides a simple, reliable, and self-calibration method for absolute concentration measurements. The instrument is suitable for long-term stable operation and requires minimal maintenance. Also, by setting different modulation frequencies, multiple lasers can be mixed to achieve simultaneous detection at multiple wavelengths using only one cavity and one detector. In particular, this method will play an important role in multiple wavelength-dependent optical parameters measurement.⁵⁰ Custom-developed lock-in circuits could replace the commercial lock-in amplifier, reducing the instrument cost and promoting a wider range of applications to NO_2 and other species.

AUTHOR INFORMATION

Corresponding Author

* Tel.: +86-551-65591961; Fax: +86-551-65591560; E-mail: wxzhao@aiofm.ac.cn (W. Zhao).

* E-mail: wjzhang@aiofm.ac.cn (W. Zhang).

ORCID

Weixiong Zhao: 0000-0003-1700-8992

Dean S. Venables: 0000-0002-4135-1793

Weidong Chen: 0000-0001-6141-1039

Notes

The authors declare no competing financial interest.

ACKNOWLEDGMENT

This research is supported by the National Natural Science Foundation of China (42022051, U21A2028, 41627810), the Second Tibetan Plateau Scientific Expedition and Research program (2019QZKK0606), the Youth Innovation Promotion Association CAS (Y202089), the Instrument Developing Project of the Chinese Academy of Sciences (YJKYYQ20180049), and the HFIPS Director's Fund (YZJJ202101, BJPY2019B02).

REFERENCES

(1) *Chemistry of the upper and lower atmosphere: theory, experiments, and applications*; Finlayson-Pitts, B. J., Pitts, J. N.; Academic Press, 2000; pp 264-293.

(2) *Atmospheric chemistry and physics: from air pollution to climate change*; Seinfeld, J. H., Pandis, S. N.; John Wiley & Sons, Inc., 2006; pp 36-38.

(3) Atkinson, R. Atmospheric chemistry of VOCs and NO_x, *Atmos. Environ.* **2000**, *34*, 2063-2101.

(4) Crutzen, P. J. The role of NO and NO₂ in the chemistry of the troposphere and stratosphere, *Ann. Rev. Earth Planet. Sci.* **1979**, *7*, 443-472.

(5) Brown, S. S. Absorption spectroscopy in high-finesse cavities for atmospheric studies, *Chem. Rev.* **2003**, *103*, 5219-5238.

(6) Ruth, A. A.; Dixneuf, S.; Raghunandan, R. Broadband cavity-enhanced absorption spectroscopy with incoherent light, In *Cavity-Enhanced Spectroscopy and Sensing*, Gagliardi, G.; Loock, H. P. eds. Springer, Berlin, Heidelberg, 2014.

(7) Hargrove, J.; Zhang, J. Measurements of NO_x, acyl peroxy nitrates, and NO₂ with automatic interference corrections using a NO₂ analyzer and gas phase titration, *Rev. Sci. Instrum.* **2008**, *79*, 046109.

(8) Paul, D.; Osthoff, H. D. Absolute measurements of total peroxy nitrate mixing ratios by thermal dissociation blue diode laser cavity ring-down spectroscopy, *Anal. Chem.* **2010**, *82*, 6695-6703.

(9) Thaler, R. D.; Mielke, L. H.; Osthoff, H. D. Quantification of nitril chloride at part per trillion mixing ratios by thermal dissociation cavity ring-down spectroscopy, *Anal. Chem.* **2011**, *83*, 2761-2766.

(10) Thieser, J.; Schuster, G.; Schuladen, J.; Phillips, G. J.; Reiffs, A.; Parchatka, U.; Pöhler, D.; Lelieveld, J.; Crowley, J. N. A two-channel thermal dissociation cavity ring-down spectrometer for the detection of ambient NO₂, RO₂NO₂ and RONO₂, *Atmos. Meas. Tech.* **2016**, *9*, 553-576.

(11) Sadanaga, Y.; Takaji, R.; Ishiyama, A.; Nakajima, K.; Matsuki, A.; Bandow, H. Thermal dissociation cavity attenuated phase shift spectroscopy for continuous measurement of total peroxy and organic nitrates in the clean atmosphere, *Rev. Sci. Instrum.* **2016**, *87*, 074102.

(12) Keehan, N. I.; Brownwood, B.; Marsavin, A.; Day, D. A.; Fry, J. L. A thermal-dissociation-cavity ring-down spectrometer (TD-CRDS) for the detection of organic nitrates in gas and particle phases, *Atmos. Meas. Tech.* **2020**, *13*, 6255-6269.

(13) Friedrich, N.; Tadic, I.; Schuladen, J.; Brooks, J.; Darbyshire, E.; Drewnick, F.; Fischer, H.; Lelieveld, J.; Crowley, J. N. Measurement of NO_x and NO_y with a thermal dissociation cavity ring-down spectrometer (TD-CRDS): instrument characterisation and first deployment, *Atmos. Meas. Tech.* **2020**, *13*, 5739-5761.

(14) Li, C.; Wang, H.; Chen, X.; Zhai, T.; Chen, S.; Li, X.; Zeng, L.; Lu, K. Thermal dissociation cavity-enhanced absorption spectrometer for measuring NO₂, RO₂NO₂, and RONO₂ in the atmosphere, *Atmos. Meas. Tech.* **2021**, *14*, 4033-4051.

(15) Liu, Y.; Morales-cueto, R.; Hargrove, J.; Medina, D.; Zhang, J. Measurements of peroxy radicals using chemical amplification-cavity ringdown spectroscopy, *Environ. Sci. Technol.* **2009**, *43*, 7791-7796.

(16) George, M.; Andrés Hernández, M. D.; Nenakhov, V.; Liu, Y.; Burrows, J. P. Airborne measurement of peroxy radicals using chemical amplification coupled with cavity ring-down spectroscopy: the PeRCEAS instrument, *Atmos. Meas. Tech.* **2020**, *13*, 2577-2600.

(17) Horstjann, M.; Andrés Hernández, M. D.; Nenakhov, V.; Chrobry, A.; Burrows, J. P. Peroxy radical detection for airborne atmospheric measurements using absorption spectroscopy of NO₂, *Atmos. Meas. Tech.* **2014**, *7*, 1245-1257.

(18) Wood, E. C.; Charest, J. R. Chemical amplification - cavity attenuated phase shift spectroscopy measurements of atmospheric peroxy radicals, *Anal. Chem.* **2014**, *86*, 10266-10273.

(19) Chen, Y.; Yang, C.; Zhao, W.; Fang, B.; Xu, X.; Gai, Y.; Lin, X.; Chen, W.; Zhang, W. Ultra-sensitive measurement of peroxy radicals by chemical amplification broadband cavity-enhanced spectroscopy, *Analyst* **2016**, *141*, 5870-5878.

(20) Fuchs, H.; Dubé, W. P.; Lerner, B. M.; Wagner, N. L.; Williams, E. J.; Brown, S. S. A sensitive and versatile detector for atmospheric NO₂ and NO_x based on blue diode laser cavity ring-down spectroscopy, *Environ. Sci. Technol.* **2009**, *43*, 7831-7836.

(21) Wagner, N. L.; Dubé, W. P.; Washenfelder, R. A.; Young, C. J.; Pollack, I. B.; Ryerson, T. B.; Brown, S. S. Diode laser-based cavity ring-down instrument for NO₃, N₂O₅, NO, NO₂ and O₃ from aircraft, *Atmos. Meas. Tech.* **2011**, *4*, 1227-1240.

(22) Perring, A. E.; Pusede, S. E.; Cohen, R. C. An observational perspective on the atmospheric impacts of alkyl and multifunctional nitrates on ozone and secondary organic aerosol, *Chem. Rev.* **2013**, *113*, 5848-5870.

(23) Monks, P. S. Gas-phase radical chemistry in the troposphere, *Chem. Soc. Rev.* **2005**, *34*, 376-395.

(24) Lu, K.; Guo, S.; Tan, Z.; Wang, H.; Shang, D.; Liu, Y.; Li, X.; Wu, Z.; Hu, M.; Zhang, Y. Exploring atmospheric free-radical chemistry in China: the self-cleansing capacity and the formation of secondary air pollution, *Natl. Sci. Rev.* **2019**, *6*, 579-594.

(25) Keller-Rudek, H.; Moortgat, G. K.; Sander, R.; Sørensen, R. The MPI-Mainz UV/VIS spectral atlas of gaseous molecules of atmospheric interest, *Earth Syst. Sci. Data* **2013**, *5*, 365-373.

(26) Wada, R.; Orr-Ewing, A. J. Continuous wave cavity ring-down spectroscopy measurement of NO₂ mixing ratios in ambient air, *Analyt* **2005**, *130*, 1595-1600.

(27) Kebabian, P. L.; Herndon, S. C.; Freedman, A. Detection of nitrogen dioxide by cavity attenuated phase shift spectroscopy, *Anal. Chem.* **2005**, *77*, 724-728.

(28) Wojtas, J.; Czyzewski, A.; Staciewicz, T.; Bielecki, Z. Sensitive detection of NO₂ with cavity enhanced spectroscopy, *Opt. Appl.* **2006**, *36*, 461-467.

(29) Courtillot, I.; Morville, J.; Motto-ros, V.; Romanini, D. Sub-ppb NO₂ detection by optical feedback cavity-enhanced absorption spectroscopy with a blue diode laser, *Appl. Phys. B* **2006**, *85*, 407-412.

(30) Grilli, R.; Méjean, G.; Kassi, S.; Ventrillard, I.; Abd-Alrahman C.; Romanini, D. Frequency comb based spectrometer for in situ and real time measurements of IO, BrO, NO₂, and H₂CO at pptv and ppqv levels, *Environ. Sci. Technol.* **2012**, *46*, 10704-10710.

(31) Fang, B.; Zhao, W.; Xu, X.; Zhou, J.; Ma, X.; Wang, S.; Zhang, W.; Venables, D. S.; Chen, W. Portable broadband cavity-enhanced spectrometer utilizing Kalman filtering: application to real-time, in situ monitoring of glyoxal and nitrogen dioxide, *Opt. Express* **2017**, *25*, 26910-26922.

- (32) Hu, S. M. Trace gas measurements using cavity ring-down spectroscopy, In *Advances in spectroscopic monitoring of the atmosphere*, Chen, W.; Venables, D. S.; Sigrist, M. W. eds. Elsevier, 2021.
- (33) Ouyang, B.; Jones, R. L. Understanding the sensitivity of cavity-enhanced absorption spectroscopy: pathlength enhancement versus noise suppression, *Appl. Phys. B* **2012**, 109, 581–591.
- (34) Long, D. A.; Cygan, A.; van Zee, R. D.; Okumura, M.; Miller, C. E.; Lisak, D.; Hodges, J. T. Frequency-stabilized cavity ring-down spectroscopy, *Chem. Phys. Lett.* **2012**, 536, 1-8.
- (35) Ye, J.; Ma, L. S.; Hall, J. L. Ultrasensitive detections in atomic and molecular physics: demonstration in molecular overtone spectroscopy, *J. Opt. Soc. Am. B* **1998**, 15, 6-15.
- (36) Zhao, W.; Gao, X.; Chen, W.; Zhang, W.; Huang, T.; Wu, T.; Cha, H. Wavelength modulated off-axis integrated cavity output spectroscopy in the near infrared, *Appl. Phys. B* **2007**, 86, 353-359.
- (37) Baer, D. S.; Paul, J. B.; Gupta, M.; O’Keefe, A. O. Sensitive absorption measurements in the near-infrared region using off-axis integrated-cavity-output spectroscopy, *Appl. Phys. B* **2002**, 75, 261-265.
- (38) Ayers, J. D.; Apodaca, R. L.; Simpson, W. R.; Baer, D. S. Off-axis cavity ringdown spectroscopy: application to atmospheric nitrate radical detection, *Appl. Opt.* **2005**, 44, 7239-7242.
- (39) Karpf, A.; Qiao, Y.; Rao, G. N. Ultrasensitive, real-time trace gas detection using a high-power, multimode diode laser and cavity ringdown spectroscopy, *Appl. Opt.* **2016**, 55, 4497-4504.
- (40) Chan, M. C.; Yeung, S. H. High-resolution cavity enhanced absorption spectroscopy using phase-sensitive detection, *Chem. Phys. Lett.* **2003**, 373, 100–108.
- (41) Scofield, J. H. A frequency-domain description of a lock-in amplifier, *Am. J. Phys.* **1994**, 62, 129-133.
- (42) About lock-in amplifiers, application note #3, SRS Home Page. www.thinkSRS.com (accessed 26 November 2021).
- (43) Großkloß, R.; Kersten, P.; Demtröder, W. Sensitive amplitude- and phase-modulated absorption-spectroscopy with a continuously tunable diode laser, *Appl. Phys. B* **1994**, 58, 137-142.
- (44) Zhao, W.; Dong, M.; Chen, W.; Gu, X.; Hu, C.; Gao, X.; Huang, W.; Zhang, W. Wavelength-resolved optical extinction measurements of aerosols using broad-band cavity-enhanced absorption spectroscopy over the spectral range of 445-480 nm, *Anal. Chem.* **2013**, 85, 2260-2268.
- (45) Vandaele, A. C.; Hermans, C.; Fally, S.; Carleer, M.; Colin, R.; Mérianne, M. F.; Jenouvrier, A. High-resolution Fourier transform measurement of the NO₂ visible and near-infrared absorption cross-sections: Temperature and pressure effects, *J. Geophys. Res.* **2002**, 107, 4348.
- (46) Volkamer, R.; Spietz, P.; Burrows, J. P.; Platt, U. High-resolution absorption cross-section of glyoxal in the UV-vis and IR spectral ranges, *J. Photochem. Photobiol. A: Chem.* **2005**, 172, 35-46.
- (47) Meller, R.; Raber, W.; Crowley, J. N.; Jenkin, M. E.; Moortgat, G. K. The UV-visible absorption spectrum of methylglyoxal, *J. Photochem. Photobiol. A: Chem.* **1991**, 62, 163-171.
- (48) Hargrove, J.; Wang, L.; Muyskens, K.; Muyskens, M.; Medina, D.; Zaide, S.; Zhang, J. Cavity ring-down spectroscopy of ambient NO₂ with quantification and elimination of interferences, *Environ. Sci. Technol.* **2006**, 40, 7868-7873.
- (49) Min, K. E.; Washenfelder, R. A.; Dubé, W. P.; Langford, A. O.; Edwards, P. M.; Zarzana, K. J.; Stutz, J.; Lu, K.; Rohrer, F.; Zhang, Y.; Brown, S. S. A broadband cavity enhanced absorption spectrometer for aircraft measurements of glyoxal, methylglyoxal, nitrous acid, nitrogen dioxide, and water vapor, *Atmos. Meas. Tech.* **2016**, 9, 423-440.
- (50) Xu, X.; Zhao, W.; Fang, B.; Zhou, J.; Wang, S.; Zhang, W.; Venables, D. S.; Chen, W. Three-wavelength cavity-enhanced albedometer for measuring wavelength-dependent optical properties and single-scattering albedo of aerosols, *Opt. Express* **2018**, 26, 33484-33500.

Figure for TOC only

